NASA TECHNICAL NOTE

NASA TN D-5015

c. 1

NASA TN D-5015

MEASUREMENT OF LIQUID AND TWO-PHASE HYDROGEN DENSITIES WITH A CAPACITANCE DENSITY METER

by George E. Turney and Roger W. Snyder

Lewis Research Center
Cleveland, Ohio

NATIONAL AERONAUTICS AND SPACE ADMINISTRATION • WASHINGTON, D. C. • APRIL 1969

MEASUREMENT OF LIQUID AND TWO-PHASE HYDROGEN DENSITIES WITH A CAPACITANCE DENSITY METER

By George E. Turney and Roger W. Snyder

Lewis Research Center
Cleveland, Ohio

NATIONAL AERONAUTICS AND SPACE ADMINISTRATION

For sale by the Clearinghouse for Federal Scientific and Technical Information
Springfield, Virginia 22151 – CFSTI price $3.00

ABSTRACT

A three-dimensional, wire matrix, capacitance density meter was used to measure the density of liquid and two-phase hydrogen flow. The measurements were made in a 4-inch (10.16-cm) nominal diameter propellant feedline of a full-scale, simulated, nuclear-rocket test system. An evaluation of this capacitance density meter was made by comparing the density meter measurements with corresponding calculated densities in the feedline. The local hydrogen densities measured with the density meter were in relatively close agreement with the calculated densities. For the most part, the calculated and measured densities differed by less than ±15 percent of the full-scale (liquid hydrogen) density.

MEASUREMENT OF LIQUID AND TWO-PHASE HYDROGEN DENSITIES WITH A CAPACITANCE DENSITY METER

by George E. Turney and Roger W. Snyder

Lewis Research Center

SUMMARY

A three-dimensional, wire matrix, capacitance density meter was used to measure the density of two-phase and liquid-hydrogen flow. The measurements were made in a 4-inch (10.16-cm) nominal diameter propellant feedline of a full-scale, simulated, nuclear-rocket test system. An evaluation of this capacitance density meter was made by comparing the density meter measurements with corresponding calculated densities in the feedline. The results of two typical test runs are presented in this report.

For the most part, the local hydrogen densities measured with the density meter were in relatively close agreement with the corresponding calculated densities. Most of the calculated and measured density values differed by less than ±15 percent of the full-scale (liquid hydrogen) density. It is concluded that this type of density meter could be used to measure two-phase and liquid-hydrogen densities with an accuracy that would be acceptable in many engineering applications.

INTRODUCTION

The measurement of fluid density or vapor content in flowing cryogenic systems is a subject of widespred interest. In the all-gas or all-liquid state, fluid density may be determined by measuring the fluid temperature and pressure and applying these measurements to an equation of state. This technique, however, cannot be used in a two-phase fluid region.

In systems that contain two-phase flow, such as the nuclear rocket, the density of the flow mixture has a significant influence on heat-transfer rates and pressure drops in the system. And, in order to analyze such two-phase flow systems, it is necessary that the local fluid densities be known.

Interest in the problem of two-phase density determination has led to the design and development of various instruments for measurement of density in croygenic flow systems. The more promising of the many techniques proposed are based on either (1) measurement of the nuclear radiation attenuation properties of the fluid or (2) measurement of the average dielectric constant or capacitance of the fluid. In theory, both these measurable quantities are related to the fluid density.

At the Lewis Research Center, considerable experience in density measurement has been gained from tests in which a capacitance density meter was used. In this report, results obtained from tests made with a meter using a three-dimensional, wire matrix, capacitance transducer are presented. A detailed description of this density meter is given in the section, DISCUSSION OF CAPACITANCE DENSITY METER.

The capacitance transducer of this density meter was installed in the downstream end of the propellant transfer line (feedline) of a full-scale simulated nuclear-rocket test system. The meter was used to measure the local density of hydrogen in the propellant feedline during cold-flow startup experiments. The simulated nuclear-rocket test system in which this meter was used is located at the Plum Brook Station of the Lewis Research Center. (Ref. 1 has a detailed description of the system.)

The propellant feedline of the test system was instrumented so that the rate of heat transfer to the hydrogen flow during startup could be calculated directly from experimental measurements. The local hydrogen densities were computed by numerically integrating the continuity and energy equations along the length of the propellant feedline. The calculated heat inputs, measured pressures, and measured inlet flow rates of the feedline were used in the density calculations.

An evaluation of the capacitance density meter was made by comparing the density meter measurements with calculated local densities in the feedline. The measured and calculated local densities for two startup tests (runs 8 and 15) are presented and compared in this report.

SYMBOLS

A	free flow area, ft^2; cm^2
α	coefficient in dielectric coefficient equation (eq. (5)), pF
A_{T_c}	dielectric coefficient (temperature dependent) (eq. (4)), pF
B	capacitance temperature coefficient due to expansion of matrix (eq. (5)), pF/^{o}R; pF/K
C	total capacitance, pF

C_p	specific heat of fluid at constant pressure, Btu/(lb_{mass})(^oR); J/(g)(K)
C_s	stray capacitance, pF
C_{ref}	total capacitance at a particular reference condition, pF
C_ϵ	capacitance due to dielectric fluid in matrix, pF
C_0	capacitance of evacuated matrix assembly (eq. (8)), pF
c	heat capacity of stainless steel feedline, Btu/(lb_{mass})(^oR); J/(g)(K)
D	$(C - C_{ref}) - (C_o - C_{ref})$
h	enthalpy of fluid, Btu/lb_{mass}; J/g
J	mechanical equivalent of heat equal to 778 (ft)(lb_{force})/Btu (100 N-cm/J)
K	conversion factor (eq. (15)), equal to 144 $in.^2/ft^2$ (10^{-4} m^2/cm^2)
L	length of flow element (eq. (A14)) ft; cm
M	mass of feedline (eq. (23)), lb_{mass}; g
$\mathcal{M}$	molecular weight, g/(g)(mole)
m	fluid mass, lb_{mass}; g
N	Avogadro's number, 6.02×10^{23} molecules/(g)(mole)
P	static pressure, $lb_{force}/in.^2$ abs; N/m^2
p	specific polarization, ft^3/lb_{mass}; cm^3/g
$\dot{Q}'$	rate of heat input to fluid per unit length of flow passage, Btu/(sec)(ft); J/(cm)(sec)
$\dot{Q}_T$	rate of heat input to fluid from feedline inlet to feedline outlet (eq. (A20)) Btu/sec; J/sec
T	temperature, ^oR; K
T_c	temperature of matrix, ^oR; K
V	volume of a flow element (eq. (A13)) ft^3; cm^3
v	velocity, ft/sec; cm/sec
X	ratio of mass flow rate of gas phase to total mass flow rate (eq. (A10))
x	distance or position along flow path, ft; cm
$\dot{\alpha}$	molecular effective moment induced per unit field strength, cm^3/molecules
ϵ	fraction of total liquid phase that is not converted to gas because of nonequilibrium (eq. (A11))

ε	dielectric constant
ρ	density, lb_{mass}/ft^3; g/cm^3
τ	time, sec
τ_0	zero time
$\dot{\omega}$	flow rate, lb_{mass}/sec; g/sec
Subscripts	
g	gas phase
h_i	enthalpy of fluid at feedline inlet
h_o	enthalpy of fluid at feedline outlet (feedline outlet corresponds to capacitance transducer inlet)
i	conditions at feedline inlet
j	j^{th} segment of flow passage (eq. (23))
l	liquid phase
M	local average temperature of feedline
noneq	nonequilibrium
o	conditions at feedline outlet (or capacitance transducer inlet)
P_o	static pressure at feedline outlet (feedline outlet corresponds to capacitance transducer inlet)
ref	reference condition (usually at ambient temperature and a pressure of approximately 1 psia (6.9×10^3 N/m^2))
rms	root mean square
s	static or stop action point of view (eq. (A13))
sg	saturated gas
sl	saturated liquid
superheated gas	gas at temperature above saturation temperature (eq. (A9))
w	outside surface (wall) of feedline
x	position x
(x-Δx)	position (x-Δx)
ρ_1	fluid density at condition 1

ρ_2	fluid density at condition 2
2φ	two-phase
τ	time τ
$(\tau-\Delta\tau)$	time $(\tau-\Delta\tau)$
1	condition 1
2	condition 2

DENSITY METER

The density meter described herein is composed of two major components: a three dimensional stainless-steel wire matrix capacitance transducer, and a capacitance-to-direct-current voltage converter. These two major components are described in the following subsections.

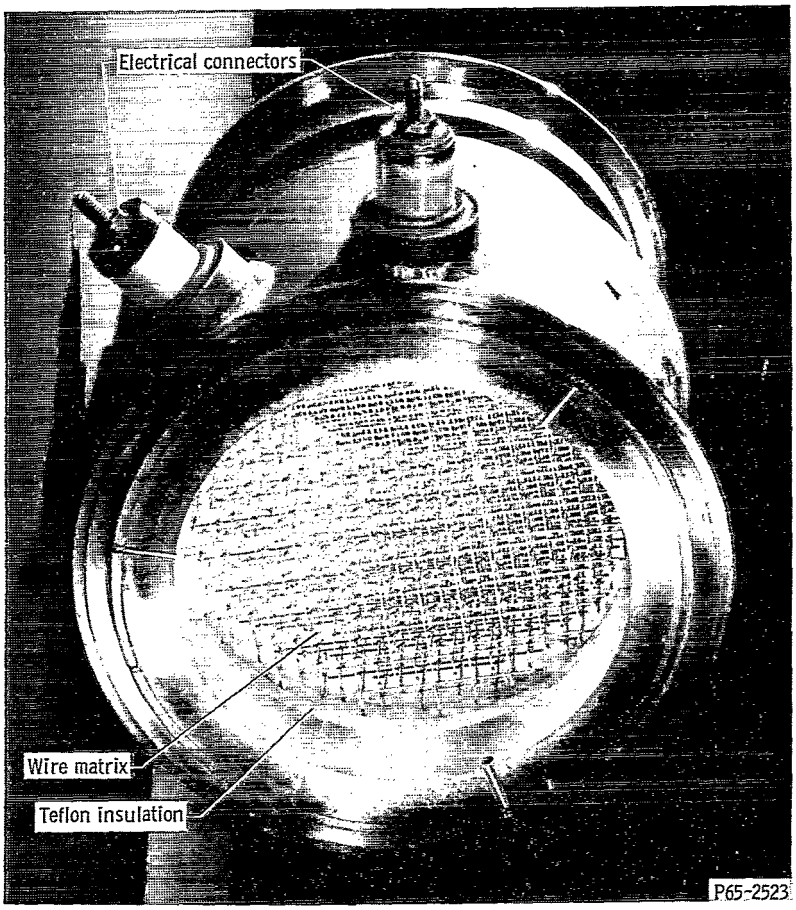

Figure 1. - Capacitance transducer.

Description of Capacitance Transducer

A photograph of the capacitance transducer is shown in figure 1. This wire matrix capacitor was designed and built by Space Science, Inc. (now Ikor Inc., Burlington, Mass.). A sketch of the wire matrix capacitor is shown in figure 2.

The assembly (fig. 2) consists of two electrically isolated three-dimensional wire matrices, each centered in the lattice of the other. (Solid and dashed lines are used in fig. 2 to represent the respective matrices.) The spacing between lattices is held fixed by a Teflon retainer ring. The three-dimensional matrix is mounted inside a pipe section and the electrical leads are brought through fittings on the pipe wall.

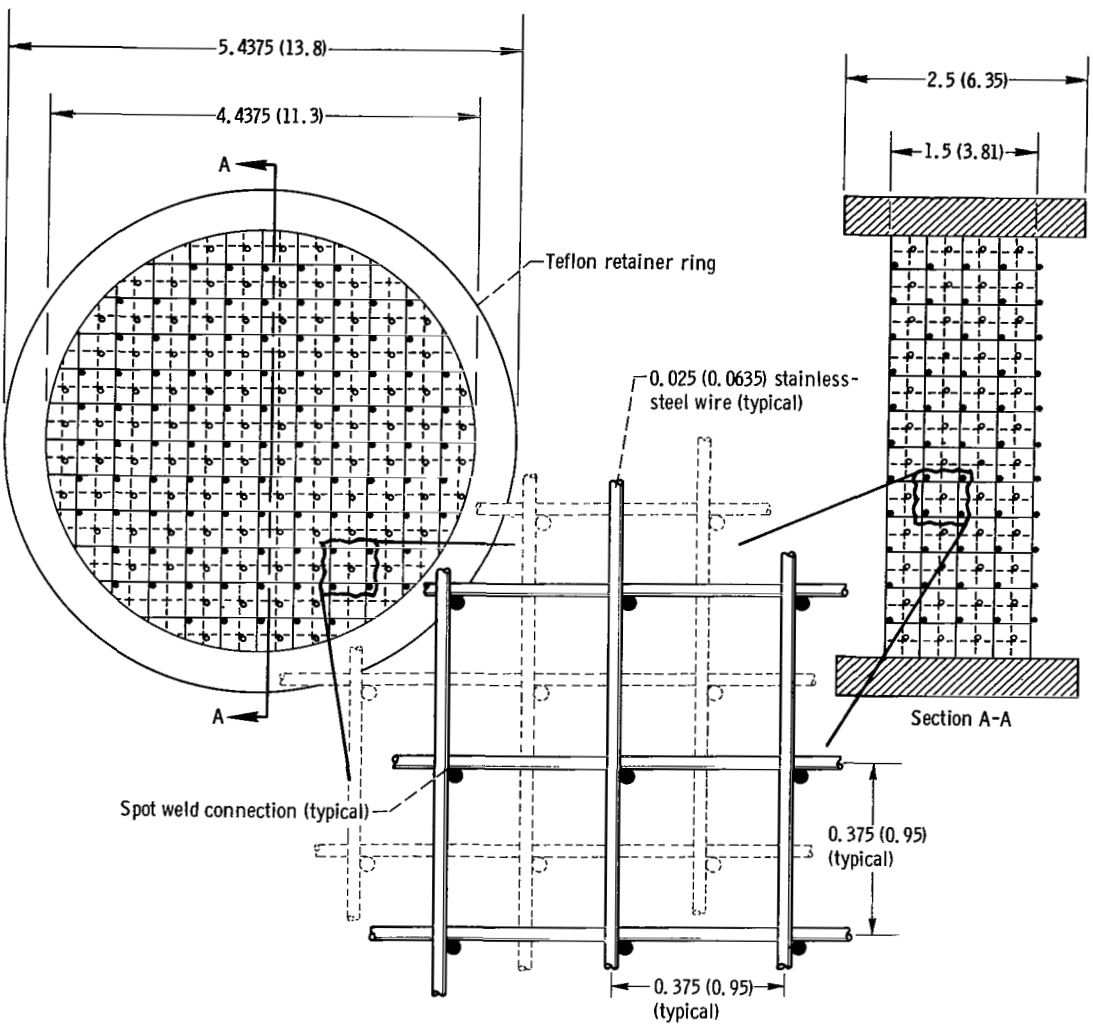

Figure 2. - Matrix assembly of capacitance - density meter. (All dimensions are in inches (cm).)

The matrix capacitor senses the average dielectric constant of the fluid flowing through the matrix volume. The matrix assembly shown in figure 2 has approximately 3200 cubical subvolumes, each with a side length of about 0.1625 inch (0.413 cm). Each of the subvolumes is equally sensitive to the fluid dielectric constant of its included mass. This is true regardless of the relative position of the subvolume in the overall sensed volume. This characteristic makes the matrix sensor insensitive to fluid inhomogeneities, bubble position, or zero gravity.

The density measured by the density meter is a static or "stop-action" density; that is, the measured density is the ratio of mass of fluid contained in the matrix to the volume of the matrix. In the appendix, it is shown that the static or stop-action density of a two-phase flow mixture is equivalent to the so-called "mixing-cup" density when the velocities of the gas and liquid phases are equal. The mixing-cup density is defined as the ratio of total mass flow rate to the total volumetric flow rate.

Description of Electronics

The electronics for this density meter consists of a standard type of capacitance to direct-current (dc) voltage converter. A simplified illustration of a typical density meter installation is shown in figure 3. The dc voltage converter contains a radio-frequency (RF) oscillator, which is a transformer coupled to an inductance-capacitance (LC) bridge.

The inductances of the bridge consist of autotransformers for coarse zero and span adjustments. One of the two capacitance legs includes the matrix capacitor. The other

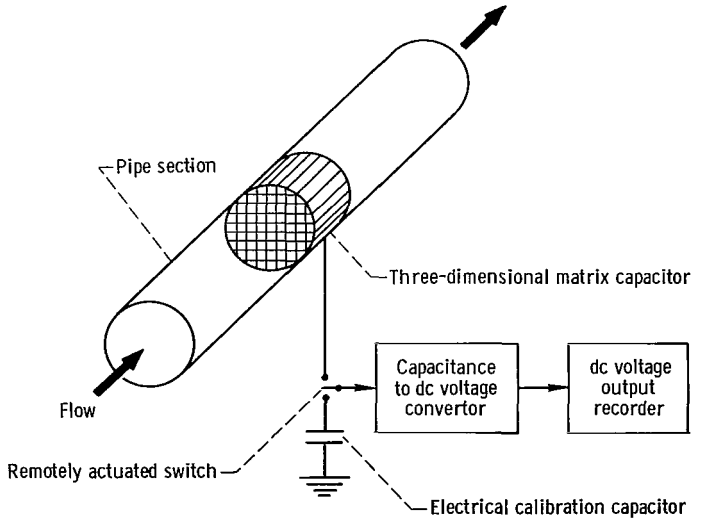

Figure 3. - Simplified illustration of density meter installation.

capacitance leg is a reference capacitor which is adjusted to balance the matrix capacitance. The output of the bridge is a signal proportional to the unbalance between the matrix and the reference capacitances.

The capacitance to dc voltage converter was modified somewhat to accept a remotely acutated electrical calibration signal by substituting a predetermined electrical calibration capacitor in place of the matrix capacitance.

The density meter tested at Lewis had the following characteristics:

(1) Range, 0 to 5 pounds mass per cubic foot (0 to 0.008 g/cm^3) in liquid hydrogen

(2) Accuracy, ±0.10 pound mass per cubic foot (±0.00016 g/cm^3) in liquid hydrogen

(3) Hydrodynamic response time, 0.63 (volume matrix) $\rho/\dot{\omega}$

(4) Electronic response time, <0.01 second

(5) Temperature effect, 2-percent shift in capacitance from 540° to 36° R (300° to 20° K)

(6) Zero capacitance, 130 picofarads

(7) Delta capacitance, 30 picofarads (gas to liquid hydrogen)

(8) Transducer pipe size, 4 inch (10 cm) nominal schedule 40

(9) Flow blockage, 13 percent of transducer pipe area

Density Equation

An equation relating density to the dielectric constant of a substance can be derived from classical electrostatic theory (see refs. 2 and 3). The equation, commonly referred to as the Clausius-Mossotti equation, is as follows.

$$\rho = \frac{1}{\left(\frac{4\pi}{3}\frac{N\alpha}{\mathcal{M}}\right)}\frac{\varepsilon - 1}{\varepsilon + 2} \tag{1}$$

The quantity inside the parentheses in equation (1) is called the specific polarization. For a particular substance, if α is constant, the specific polarization of the substance is constant, and the substance is said to obey the Clausius-Mossotti equation. Equation (1) was derived making use of the following assumptions:

(1) Molecules are nonpolar and spherical.

(2) No short-range interactions occur between molecules.

(3) Molecules have isotropic spatial distribution.

Although hydrogen meets none of these assumptions exactly over the entire range of densities, investigators have found that the specific polarization of hydrogen is essentially constant. Table I lists the values of specific polarization for hydrogen obtained by

TABLE I. - VALUES OF SPECIFIC POLARIZATION OF HYDROGEN

Researchers	Reference	Hydrogen state	Temperatures, K	Approximate range of specific volumes, cm^3/g	Specific polarization, p, cm^3/g
Werner and Keesom	8	Liquid	14 to 20.4	13 to 14	1.010±0.002
Guillien	9	↓	14 to 20.4	13 to 14	.9984±0.002
van Itterbeek and Spaepen	10	↓	20.4	14	.988±0.003
Johns and Wilhelm	11	↓	20.4	14	.9986±0.001
Maryott and Buckley	12	Gas	293	12 000	1.0104±0.002
Michels, et al.	13	Gas	298 and 373	16 to 11 000	1.001±0.002

different investigators. Regardless of the state of the hydrogen, the specific polarization (table I) equalled 1.00 cubic centimeter per gram to within ±1 percent.

Hust, et al., (ref. 4) show that the dielectric constant of hydrogen depends only on fluid density, regardless of fluid phase. They report the dielectric constant of para-hydrogen for the range 24 to 100 K with densities from 0.005 to 0.080 gram per cubic centimeter.

Therefore, the Clausius-Mossotti equation, which is sufficient to cover all three states of hydrogen, is

$$\rho = \frac{1}{p}\,\frac{\varepsilon - 1}{\varepsilon + 2} \tag{2}$$

where

$$p = \left(\frac{4\pi}{3}\,\frac{N\alpha}{\mathcal{M}}\right) = \text{constant} = 1.00\ cm^3/g$$

Equation (2) indicates that, for a constant specific polarization p, the fluid density is a unique function of the dielectric constant. And the average dielectric constant of the fluid is directly related to the capacitance. As a result of these relations, fluid density can be determined from capacitance measurements.

The total capacitance of the three-dimensional assembly C is the sum of the stray capacitance C_s and the capacitance of the dielectric fluid in the matrix C_ε. Expressed as an equation,

$$C = C_s + C_\varepsilon \tag{3}$$

The capacitance due to the dielectric fluid in the matric C_ε is directly proportional to the dielectric constant of the fluid; that is,

$$C_\varepsilon = \mathcal{A}_{T_c} \varepsilon \tag{4}$$

The dielectric coefficient $\mathcal{A}_{T_c}$ is a function of the matrix dimensions. And these dimensions change slightly with the matrix temperature. For a constant coefficient of thermal expansion, the dielectric coefficient $\mathcal{A}_{T_c}$ is linearly proportional to the temperature of the matrix.

$$\mathcal{A}_{T_c} = (\mathscr{A} + BT_c) \tag{5}$$

By substituting the right sides of equations (4) and (5) into equation (3), the following expression for total capacitance of the matrix assembly is obtained:

$$C = (\mathscr{A} + BT_c)\varepsilon + C_s \tag{6}$$

The coefficient $\mathscr{A}$ and the temperature coefficient of the matrix B are constants that are determined from calibration tests. The methods of determining these coefficients are described later in this section.

Capacitance is a difficult quantity to measure. Our experience has been that stray capacitance is always present in undeterminable amounts during calibrations, checkouts, and tests and that it always contributes an uncertainty to any measurement that is made. For the experiments descripted herein, the stray capacitance varied as much as ±4 picofarads between tests. For hydrogen, the change in capacitance from the all gas to all liquid state is only about 30 picofarads. Consequently, the stray capacitance effect is significant.

In order to overcome this problem, a technique was derived whereby differences in capacitances were measured instead of absolute values. A reference condition must be known during the data acquistion period. Usually, this is a known single-phase point or, ideally, a point at vacuum conditions. The differences in capacitance from this reference capacitance are then measured. This technique successfully reduced stray capacitance measurement errors. To describe this technique, equation (2) is rewritten in the following equivalent form:

$$\rho = \frac{1}{p} \frac{(\varepsilon - 1)}{(\varepsilon - 1) + 3} \tag{7}$$

At perfect vacuum conditions, the dielectric constant ε is one. And the capacitance of the assembly at perfect vacuum conditions C_0 is given by

$$C_0 = (\alpha + BT_c) + C_s \tag{8}$$

If the capacitances C and C_0 are measured at a fixed matrix temperature T_c equations (6) and (8) can be combined to give the following:

$$\varepsilon = \frac{C - C_s}{C_0 - C_s} \tag{9}$$

Subtracting one from each side of equation (9) gives

$$\varepsilon - 1 = \frac{C - C_0}{C_0 - C_s} \tag{10}$$

Substituting this result into equation (7) and simplifying results in

$$\rho = \frac{1}{p} \frac{(C - C_0)}{(C - C_0) + 3(\alpha + BT_c)} \tag{11}$$

Equation (11) may be used to evaluate density if both C and C_0 are measured at the same temperature, T_c.

For the tests reported herein, it was impossible to obtain perfect vacuum conditions in the experimental setup. As a result, the absolute value of the vacuum capacitance C_0 could not be determined.

In order to obtain an equation that could be used to evaluate density, equation (11) was expressed in terms of capacitance differences, which could be determined. A known single-phase reference condition existed during the data acquisition period just before the test run. During this period, the matrix was near ambient temperature and the pressure was approximately 1 psia (6.9×10^3 N/m^2). The measured capacitance at this reference condition of low pressure and ambient temperature C_{ref} can be expressed in the following form:

$$C_{ref} = (\alpha + BT_{ref})\varepsilon_{ref} + C_s \tag{12}$$

Substracting C_{ref} from both C and C_0 in equation (11) and substituting A_{T_c} for $\alpha + BT_c$ results in an equation for density in terms of differences in capacitances:

$$\rho = \frac{1}{p}\left[\frac{(C - C_{ref}) - (C_0 - C_{ref})}{(C - C_{ref}) - (C_0 - C_{ref}) + 3A_{T_c}}\right] \tag{13}$$

As will be shown, the capacitance difference terms and the coefficient A_{T_c} in equation (13) can be readily evaluated.

The quantity $C - C_{ref}$ is the change in capacitance compared with the low pressure, ambient temperature reference condition existing before a test run. This is the quantity that is experimentally measured. The quantity $C_0 - C_{ref}$ is a correction term to account for (1) the change in the matrix dimensions due to temperature changes and (2) the nonvacuum zero conditions. This correction term is given by the following equation:

$$(C_0 - C_{ref}) = A_{T_c}(1 - \varepsilon_{ref}) + \varepsilon_{ref}B(T_c - T_{ref}) \tag{14}$$

The coefficients A_{T_c} and B in equation (14) are given by

$$A_{T_c} = \left(\frac{\frac{\partial C}{\partial \rho}}{\frac{\partial \varepsilon}{\partial \rho}}\right)_{T_c} = \left(\frac{C_{\rho_1} - C_{\rho_2}}{\varepsilon_{\rho_1} - \varepsilon_{\rho_2}}\right)_{T_c} \tag{15}$$

$$B = \left(\frac{\partial C_0}{\partial T}\right)_{\rho=0} = \left(\frac{C_{0,1} - C_{0,2}}{T_1 - T_2}\right)_{\rho=0} \tag{16}$$

The density measurement system must be calibrated to obtain numerical values for A_{T_c} and B. To determine the dielectric coefficient A_{T_c}, the capacitance is measured at two different known densities (ρ_1 and ρ_2) with the matrix at constant temperature T_c. The dielectric constants (ε_{ρ_1} and ε_{ρ_2}) in equation (15) are computed by substituting the known densities ρ_1 and ρ_2 into the Clausius-Mossotti equation. The numerical values of C_{ρ_1}, C_{ρ_2}, ε_{ρ_1}, and ε_{ρ_2} are then substituted into equation (15) to evaluate A_{T_c}.

To determine B, the capacitance of the matrix assembly is measured at two known temperatures (T_1 and T_2) with the matrix in a vacuum. The measured capacitances, $C_{0,1}$ and $C_{0,2}$ along with the known temperatures are then used in equation (16) to

evaluate the coefficient B. The density of the fluid is then obtained by substituting the numerical values of A_{T_c}, $(C - C_{ref})$, and $(C_0 - C_{ref})$ into equation (13). By an independent calibration, the value of A_{T_c} was determined to be 131.82 picofarads and the value of B was 0.00235 picofarad per ^{o}R (0.00423 pF/K).

In the appendix, the accuracy of this particular density meter is examined. And an rms inherent error for this meter is calculated to be about 3 percent (full scale) when used to measure hydrogen densities. This 3-percent error is based on the estimated uncertainties in each of the terms in equation (13).

RESEARCH APPARATUS AND PROCEDURE

The density meter was tested in a full-scale simulated nuclear-rocket test system. The full-scale test system consisted of a liquid-hydrogen storage tank, turbopump, propellant feedline, reactor, and nozzle assembly. The assembled configuration of this test system is shown in figure 4. Reference 1 provides a detailed description of the major components of this test system.

In this report, the section of propellant feedline which extends from the main discharge valve to the capacitance transducer is of major importance. The relative positions of the main discharge valve and the capacitance transducer are shown in figure 4.

Propellant Feedline

The feedline considered in this study is a 4-inch (10-cm) nominal diameter, schedule 5, AISI 304, stainless-steel pipe. This pipe has an inside diameter of 4.334 inches (11.0 cm), a wall thickness of 0.084 inch (0.213 cm), and an overall length (from main valve to capacitance density meter) of approximately 17 feet (5.2 m).

A sketch of the feedline is shown in figure 5. The capacitance transducer is shown near the discharge end of the feedline in figure 5. Two gimbal expansion joints were installed in the vertical leg of the feedline to allow movement of the line during chilldown. The entire feedline was covered with a 4-inch (10-cm) thick layer of polyurethane foam insulation. The purpose of the insulation was to minimize heat transfer to the line by free convection and to eliminate possible condensation of air on the outside surface of the pipe.

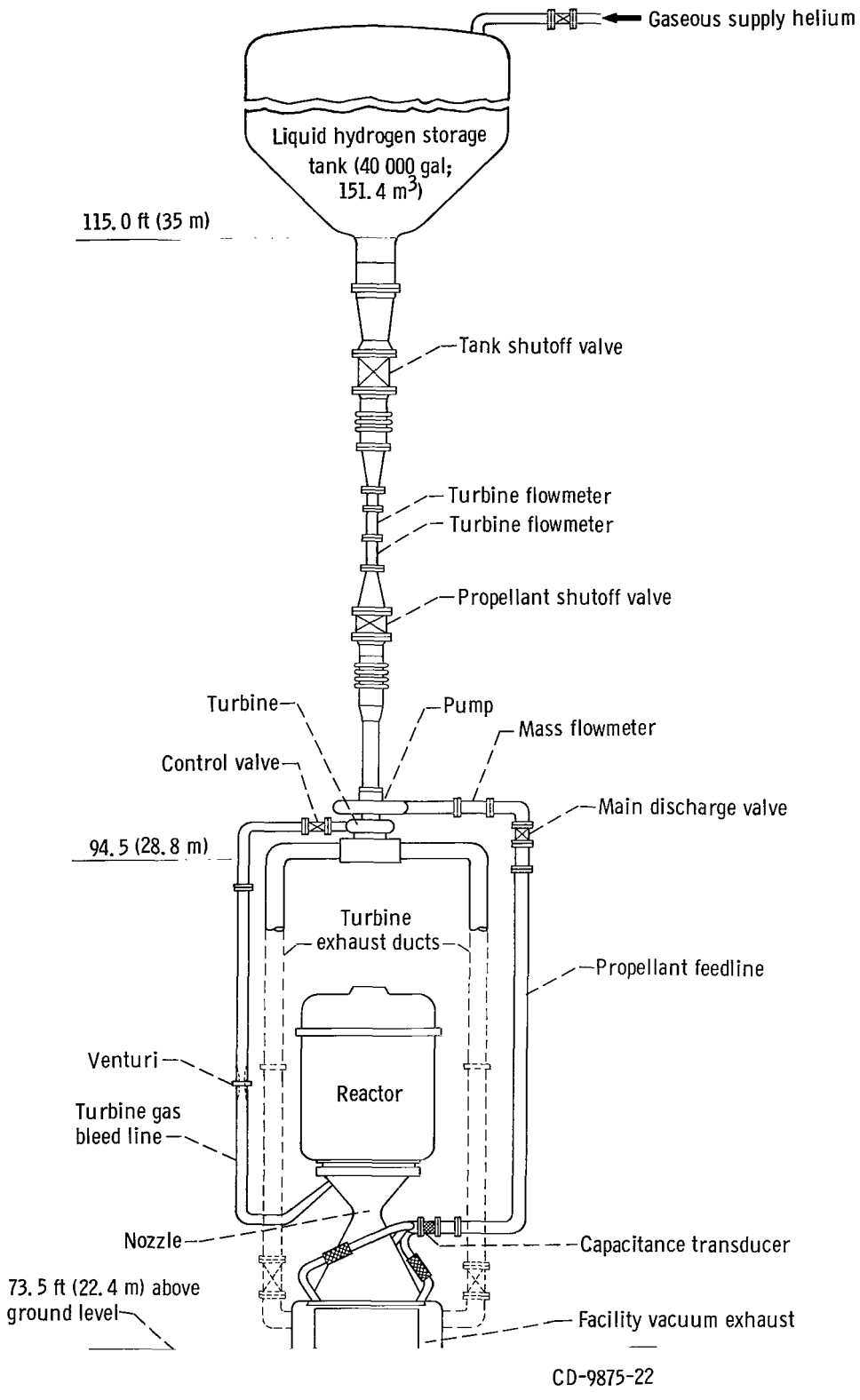

Figure 4. - Full-scale, cold-flow nuclear-rocket test system.

Coordinate	Distance from station 0	
	in.	cm
x (thermocouple)	3.03	7.70
	[a]9.06	23.0
	17.06	43.3
	29.06	73.8
	41.06	104.2
	53.06	134.8
	65.06	165.2
	74.76	190.0
	98.76	251.0
	122.76	312.0
	[a]142.56	362.0
(b)	-------	------
(c)	-------	------
y (thermocouple)	11.38	28.9
	37.38	994.9
	55.30	140.5
x (transducer[d])	16.5	41.9
	74.7	190.0
	122.7	312.0
y (transducer[d])	51.3	130.4

[a]Gimbal location.
[b]Elbow outside radius.
[c]Elbow inside radius.
[d]Range, 0 to 200 psia (13.8x10^5 N/m^2).

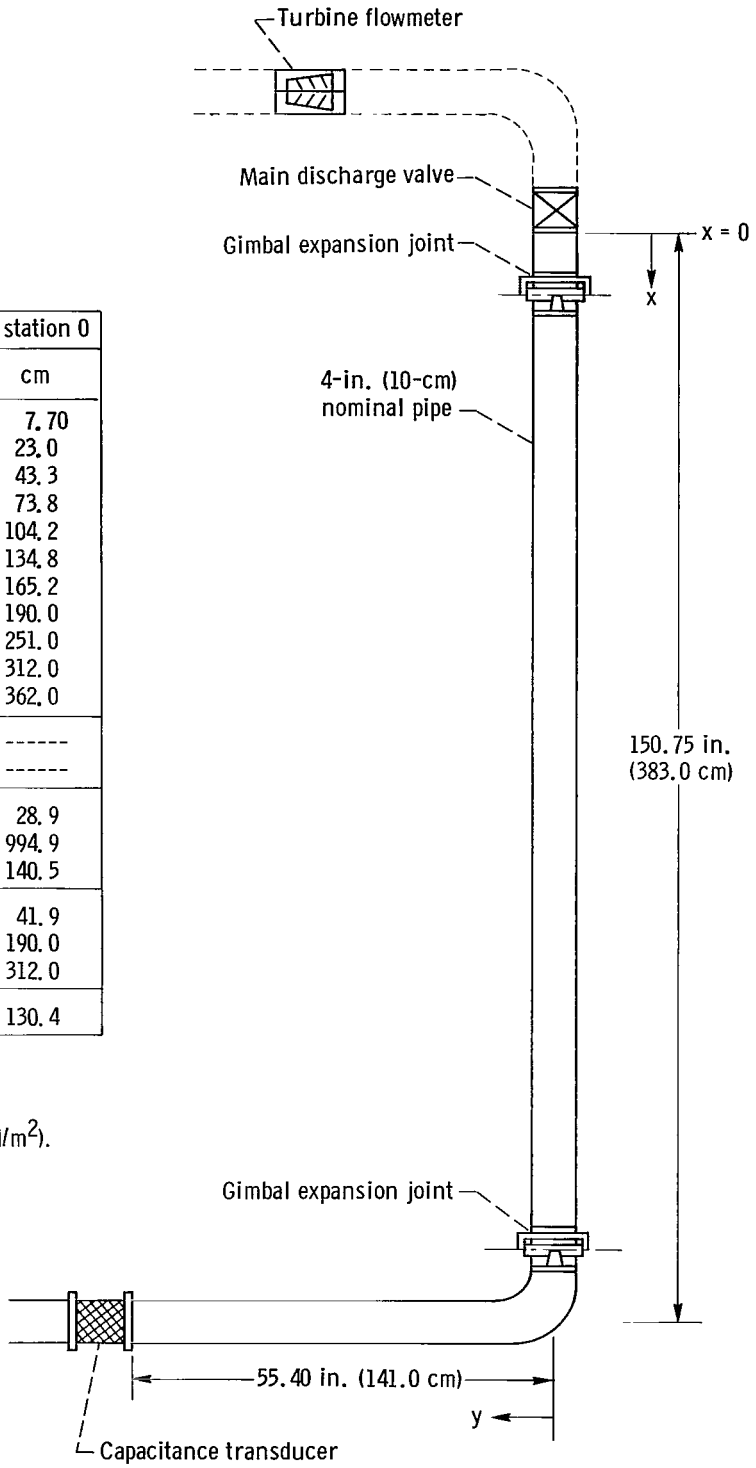

Figure 5. - Propellant feedline instrumentation.

Feedline Instrumentation and Accuracy

The locations of the pressure and material temperature measurements for the feedline are shown in figure 5. Pressures were measured at four points on the feedline with calibrated strain-gage transducers. The full-scale range of the transducers was 200 psia (13.8×10^5 N/m^2). Temperatures of the stainless-steel feedline were measured with fine wire (30 gage or 0.0255 cm diam) copper-constantan thermocouples. The measuring junctions of these thermocouples were welded to the outside wall of the feedline.

The hydrogen flow rate at the feedline inlet was measured with a turbine flowmeter. The turbine meter is shown in figure 5 just upstream of the main discharge valve.

Besides the material temperature and pressure-measurement stations listed in figure 5, other stations for the measurement of fluid temperatures and pressures were just ahead of the main discharge valve. These fluid temperatures and pressures were used to determine the enthalpy and density of the liquid hydrogen upstream of the main discharge valve. The fluid temperatures were measured with precision resistance sensors.

The estimated accuracies of the different experimental measurements are listed in table II. The accuracies listed for copper-constantan thermocouples in the range from 200° to -300° F (660° to 160° R or 367 to 89 K) were taken from the National Bureau of Standards specifications (ref. 5). For temperatures below -300° F (160° R or 89 K) the accuracy of measurements made with copper-constantan thermocouples is difficult to access. In the range from -300° to -430° F (160° to 30° R or 89 to 16.7 K), the sensitivity of copper-constantan is small. (Sensitivity as used herein is the change in thermoelectric potential with respect to temperature.) Because of the small sensitivity, measurements made with copper-constantan near the liquid-hydrogen temperature regime are appreciably affected by factors such as (1) resolution of the data recording system,

TABLE II. - INSTRUMENTATION ACCURACY

Variable	Instrument	Estimated accuracy
Flow rate	Turbine flowmeter	±2 percent of actual flow rate
Pressure	Strain-gage transducer (0 to 200 psia) (0 to 13.8×10^5 N/m^2)	±1/2 percent of full scale, i.e., ±1 psi (±6.9×10^3 N/m^2)
Fluid temperature	Resistance-type sensor	±0.50° R (±0.28 K) in temperature range from 30° to 60° R (17 - 33 K)
Material temperature	Copper-constantan thermocouple	±0.75° F (±0.42 K) for temperatures ranging from 200° to -75° F (367 to to 214 K); ±1 percent of Fahrenheit temperature from -75° to -300° F (214 to 89 K)

(2) variations in the thermoelectric powers of different wire pairs, and (3) line noise in the data acquisition system. For the tests considered in this report, the errors associated with material temperature measurements made in the liquid-hydrogen temperature region were estimated to be as much as $\pm 10^{\circ}$ R (± 5.6 K).

Test Operations

The experimental procedure used in the operation of the full-scale, simulated nuclear-rocket test system is described in reference 1. A brief summary of the processes occurring in the propellant feedline during a typical startup test is given below.

For the test runs described herein, the turbopump and piping upstream of the main discharge valve were precooled and filled with liquid hydrogen before the start of a test. The temperatures of the turbopump and piping upstream of the main valve were reduced to approximately the temperature of liquid hydrogen. The temperatures of the feedline downstream of the main discharge valve were initially near ambient temperature.

The flow of hydrogen in the feedline is initiated by a programmed opening of the main discharge valve. Time zero τ_0 corresponds to the initiation of flow by opening the main discharge valve.

In the early part of a startup test run, the feedline is near ambient temperature, and a large fraction of the liquid-hydrogen flow entering the feedline is changed to vapor as it moves downstream in the line. The hydrogen flow arriving at the capacitance transducer is therefore predominately in the vapor state. As time increases, the turbopump causes an increase in the flow and pressure in the feedline; concurrently, the temperatures of the propellant feedline decrease. As a result, less heat is transferred from the feedline to the fluid, and the density of the hydrogen arriving at the capacitance transducer increases as the run continues. Eventually, the flow exists as a subcooled liquid phase throughout the feedline.

The density meter was used to measure liquid and two-phase hydrogen densities in more than 30 bootstrap startup experiments. The range of variables covered in all the bootstrap tests, that is, the pressures, fluid temperatures, and flow rates, were nearly the same. The major difference between these bootstrap tests was in the flow-rate-time profiles. In some test runs, the feedline inlet flow rates were relatively smooth; in other runs, however, they were oscillatory, especially near the beginning of the runs. The two test runs presented in this report represent one of each of the two classes of flow-rate - time profiles. Run 15 is typical of those runs that had a smooth flow-rate profile, and run 8 is typical of those in which the flow-rate - time profile was oscillatory.

The two runs (8 and 15) were analyzed in considerable detail. Most of the other test runs were also analyzed. However, the calculational procedure used was somewhat simplified. The calculated densities obtained for these other tests were used primarily as

TABLE III. - TEST VARIABLES

Run	Length of test, sec	Flow rate range		Pressure range at feedline inlet		Fluid temperature at feedline inlet	
		lb_{mass}/sec	kg/sec	psia	kN/m^2	^oR	K
8	18	0 to 32.5	0 to 14.8	0.5 to 172	$3.45 \text{ to } 1.19 \times 10^3$	39.4 to 45.3	21.9 to 25.2
15	16	0 to 31.5	0 to 14.3	0.5 to 160	$3.45 \text{ to } 1.10 \times 10^3$	39.2 to 42.0	21.8 to 23.3

qualitative information. This information was considered, however, in the evaluation of the density meter.

For both tests (runs 8 and 15) the liquid-hydrogen storage tank was pressurized to 35 psia (2.42×10^5 N/m^2). The pressures in the feedline downstream of the main valve at τ_0 were approximately 1.0 psia (6.9×10^3 N/m^2). The important variables for runs 8 and 15 are listed in table III. The feedline inlet conditions for the two runs are presented in the section RESULTS AND DISCUSSION.

Data Acquisition and Processing

All temperature and pressure measurements in the propellant feedline were recorded on a digital multiplex system. The recorded data were then processed on a digital computer, which converted the recorded millivolt values to engineering units of temperature and pressure. A description of the data acquistion system is given in reference 1.

ANALYTICAL PROCEDURE

Consider the case of a one- or two-phase homogeneous fluid flowing in a constant area passage with heat addition. The one-dimensional differential equations of continuity and energy for nonsteady flow are written as follows:

Continuity:

$$A \frac{\partial \rho}{\partial \tau} + \frac{\partial \dot{\omega}}{\partial x} = 0 \tag{17}$$

Energy: (neglecting kinetic energy term)

$$A\rho \frac{\partial h}{\partial \tau} - \frac{AK}{J} \frac{\partial P}{\partial \tau} + \dot{\omega} \frac{\partial h}{\partial x} = \dot{Q}' \tag{18}$$

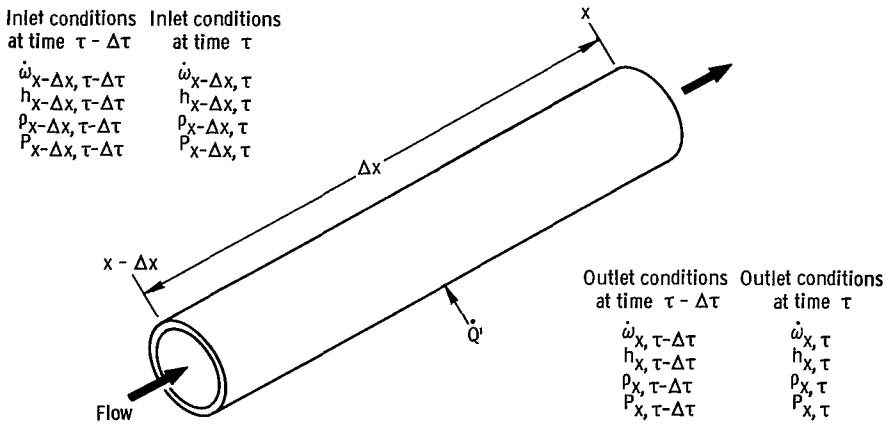

Figure 6. - Segment of propellant feedline.

Now, consider a finite segment of passage with length Δx, such as that shown in figure 6. In figure 6 there are two sets of inlet and outlet conditions: one set corresponds to time $\tau - \Delta\tau$ and the other set to time τ. If the variable designations in figure 6 are used and if a finite time interval $\Delta\tau$ is considered, the differential equations of continuity and energy (eq. (17) and (18)) can be expressed in terms of finite differences. The corresponding equations are

Continuity:

$$A \frac{\Delta_\tau \bar{\rho}}{\Delta\tau} + \frac{\Delta_x \dot{\omega}}{\Delta x} = 0 \tag{19}$$

Energy:

$$A\rho \frac{\Delta_\tau \bar{h}}{\Delta\tau} - \frac{AK\, \Delta_\tau \bar{P}}{J\, \Delta\tau} + \omega \frac{\Delta_x h}{\Delta x} = \dot{Q}' \tag{20}$$

Expanding equations (19) and (20) and using appropriate inlet and outlet values to represent averages, results in

Continuity (expanded finite difference form):

$$A\left[\frac{(\rho_{x, \tau} + \rho_{x-\Delta x, \tau}) - (\rho_{x, \tau-\Delta\tau} + \rho_{x-\Delta x, \tau-\Delta\tau})}{2\, \Delta\tau}\right] + \frac{\dot{\omega}_{x, \tau} - \dot{\omega}_{x-\Delta x, \tau}}{\Delta x} = 0 \tag{21}$$

Energy (expanded finite difference form):

$$A\frac{(\rho_{x,\tau}+\rho_{x-\Delta x,\tau})}{2}\left[\frac{(h_{x,\tau}+h_{x-\Delta x,\tau})-(h_{x,\tau-\Delta\tau}+h_{x-\Delta x,\tau-\Delta\tau})}{2\,\Delta\tau}\right]$$

$$-\frac{AK}{J}\left[\frac{(P_{x,\tau}+P_{x-\Delta x,\tau})-(P_{x,\tau-\Delta\tau}+P_{x-\Delta x,\tau-\Delta\tau})}{2\,\Delta\tau}\right]$$

$$+\frac{\dot{\omega}_{x,\tau}+\dot{\omega}_{x-\Delta x,\tau}}{2}\left[\frac{h_{x,\tau}-h_{x-\Delta x,\tau}}{\Delta x}\right]=\dot{Q}' \qquad (22)$$

The expanded finite difference forms of the continuity and energy equations were used to calculate the local fluid densities in the propellant feedline as a function of time. In applying these equations, the feedline (from main valve to capacitance transducer) was considered to be made up of 28 segments arranged in series. The average length of the segments was approximately 7.5 inches (19.05 cm). The inlet of the first segment corresponds to the position $x = 0$ in figure 5.

The heat input to each segment was determined from the stainless-steel feedline wall temperature measurements. As stated in the RESEARCH APPARATUS AND PROCEDURE section, wall temperatures were measured at 16 different stations along the length of the feedline. These temperature measurements were linearly interpolated, and an appropriate wall temperature was determined at each point in time for each of the 28 segments. In the calculations, it was assumed that the measured local wall temperatures were equal to the average local material temperatures of the feedline; that is, the temperature gradient across the feedline wall thickness was assumed to be negligible. Hence, the heat input to the fluid in time interval $\Delta\tau$ from wall segment j with length ΔX_j is given by the following equation:

$$\dot{Q}'_j=\frac{M_j}{\Delta X_j}\,\frac{\int_{T_{j,\tau-\Delta\tau}}^{T_{j,\tau}} C_j\,dT_j}{\Delta\tau} \qquad (23)$$

A similar interpolation procedure was used to determine the pressures at each point in time for the endpoints of the 28 segments.

Throughout the experimental runs, the hydrogen just ahead of the main discharge valve was subcooled (i.e., the temperature of the liquid hydrogen was below the boiling point at the existing pressure). And the enthalpy there was determined by measuring the

local fluid pressure and temperature and applying these measurements to an equation of state.

To determine the enthalpy at the inlet to the first segment, a constant enthalpy throttling process across the main discharge valve was assumed. Hence, at each point in time, the enthalpy at the inlet to the first segment was equal to the enthalpy just ahead of the main discharge valve.

The hydrogen density at the inlet to the first segment was determined as a function of time from the local enthalpy and pressure values. The following procedure was used to get the local densities, enthalpies, and flow rates in the feedline during a flow test.

Beginning with the first segment, at time zero, and considering the time interval $\Delta\tau$, the expanded finite difference forms of the continuity and energy equations were solved simultaneously. And the density, enthalpy, and flow rate at the outlet of the first segment at time τ (i.e., $\rho_{x,\tau}$, $h_{x,\tau}$, and $\dot{\omega}_{x,\tau}$) were obtained. These outlet conditions from the first segment were then assigned to the inlet of the following segment and the calculations were repeated. This stepwise procedure was continued and the fluid conditions at the outlet of each of the 28 segments at time τ were determined.

These calculations were repeated for each of the 28 segments and for each time interval $\Delta\tau$ to the end of the flow test. From these calculations, the density of hydrogen at the inlet to the capacitance transducer was determined as a function of time. (The inlet of the capacitance transducer corresponds to the outlet of segment 28.)

For the two test runs described in this report, a constant time interval of 0.2 second was used. The calculations were performed on a high-speed digital computer. The hydrogen properties used in the calculations were obtained from reference 6. Because of dependency of $\rho_{x,\tau}$ on $h_{x,\tau}$, an iterative procedure was required for the solution of the equations.

RESULTS AND DISCUSSION

Comparison of Measured and Calculated Densities

Figure 7 show the measured and calculated hydrogen densities at the feedline outlet as a function of time for runs 8 and 15. The measured and calculated traces of density for each of these tests have a similar shape. And, for the most part, the hydrogen densities measured with the capacitance density meter are considered to be in good agreement with the calculated densities.

In both of these tests, the hydrogen at the feedline outlet was a two-phase (gas-liquid) mixture for times from about 0.5 to 4.5 seconds.

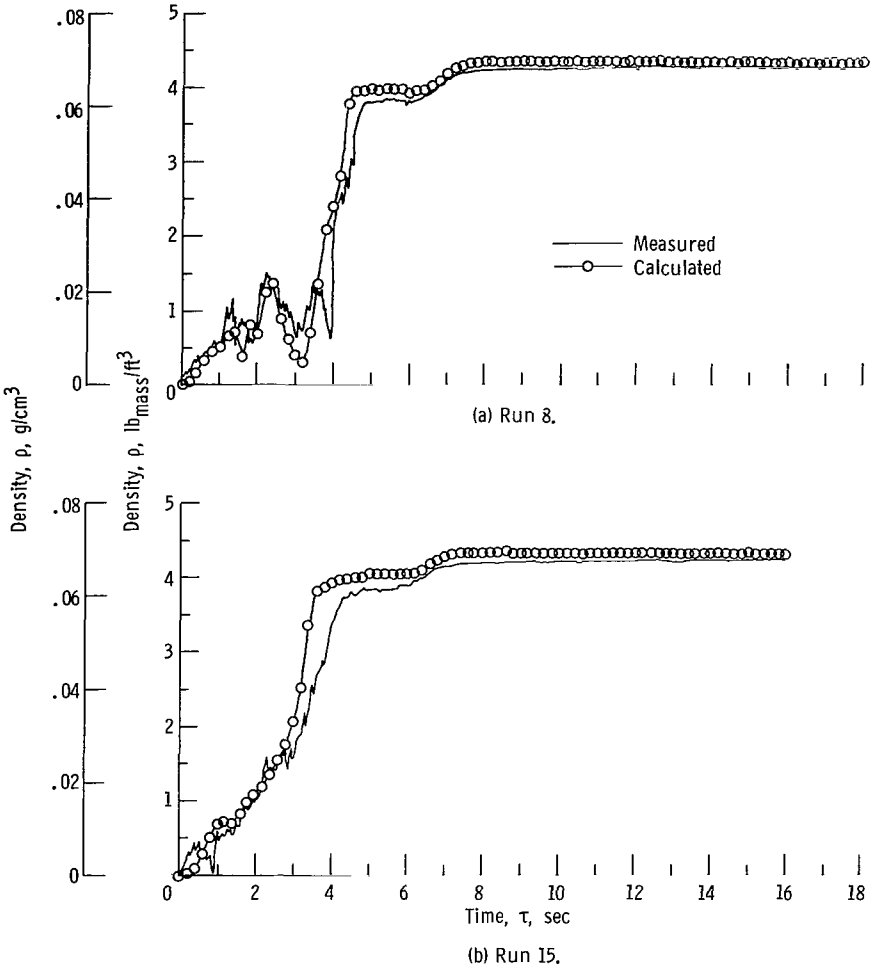

Figure 7. - Measured and calculated hydrogen density at feedline outlet as function of time.

The accuracy of the measured and calculated densities are examined in the appendix. In addition to density meter error, four important items are considered that could have a bearing on the comparisons of measured and calculated two-phase densities:

(1) Thermodynamic nonequilibrium between the gas and liquid phases

(2) Velocity differences between gas and liquid phases

(3) Possible inaccuracies in experimental measurements used in density calculations

(4) Approximations used in the determination of heat-transfer rates

The magnitude of the errors in two-phase density resulting from items (1) and (2) depends on the type of two-phase flow and the degree of turbulent mixing between the gas and liquid phases. For the test runs reported herein, no attempt was made to experimentally evaluate the temperature and velocity differences between the gas and liquid phases. Therefore, the affects of items (1) and (2) could not be quantatively accessed.

However, an indication of these individual effects on two-phase hydrogen density is given in the appendix.

For a temperature difference of 10° R (5.56 K) between the gas and liquid phases, the maximum relative error in calculated density is estimated to be about -20 percent.

And for gas-to-liquid phase velocity ratios ranging from 0.75 to 1.25, the resulting maximum relative error in calculated two-phase density is approximately ±15 percent.

The errors in calculated two-phase densities that may result from items (3) and (4) are of a systematic class. The magnitude of these possible errors are estimated in the appendix.

The maximum relative error in calculated two-phase hydrogen density due to item (3) was estimated to be approximately ±9 percent. And the maximum relative error in calculated density due to item (4) is about ±5 percent.

Most of the calculated and measured densities in figure 7 differed by less than ±15 percent of the full-scale (liquid hydrogen) density. When the possible effects of the four items discussed previously are considered, the agreement in measured and calculated densities (fig. 7) is good. For the most part the differences between calculated and measured two-phase densities are within the uncertainty band that results from the systematic errors, that is, items (3) and (4).

An important feature of this density meter is its reliability. The capacitance transducer proved to be a rugged instrument. It was installed in the propellant feedline and subjected to more than 30 transient cold-flow startup tests. After used in all these tests, there was no apparent damage to the transducer.

In this report, data for two test runs in which the density meter was used are presented. For the most part, the emphasis was placed on determining the relative accuracy of the measured local densities for these tests. It was concluded that measurements made with this density meter were relatively accurate. Information obtained from qualitative comparisons of calculated and measured densities for other test runs support this conclusion.

Input Data

The time-dependent fluid conditions at the inlet to the propellant feedline for the two test runs are shown in figures 8 to 11.

The hydrogen-inlet flow rates are shown as a function of time in figure 8. Figures 9 and 10 show the inlet fluid temperatures and pressures against time. Fluid enthalpies at the feedline inlet are shown against time in figure 11. (The differences between the solid and dashed lines in fig. 11 are a measure of the subcooling during these test runs.)

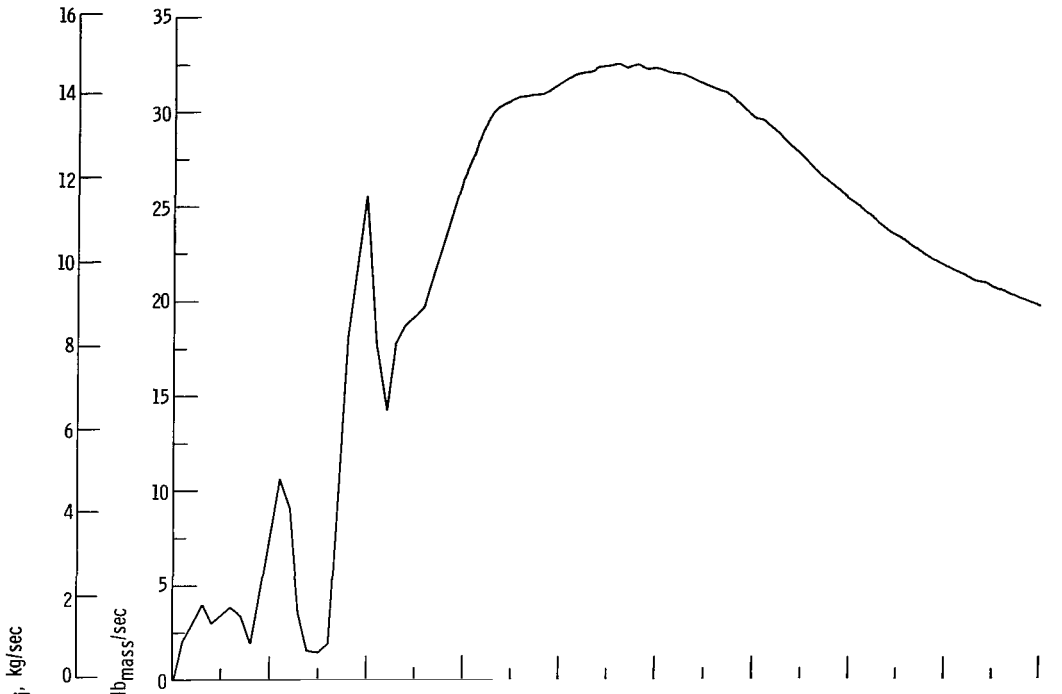

(a) Run 8.

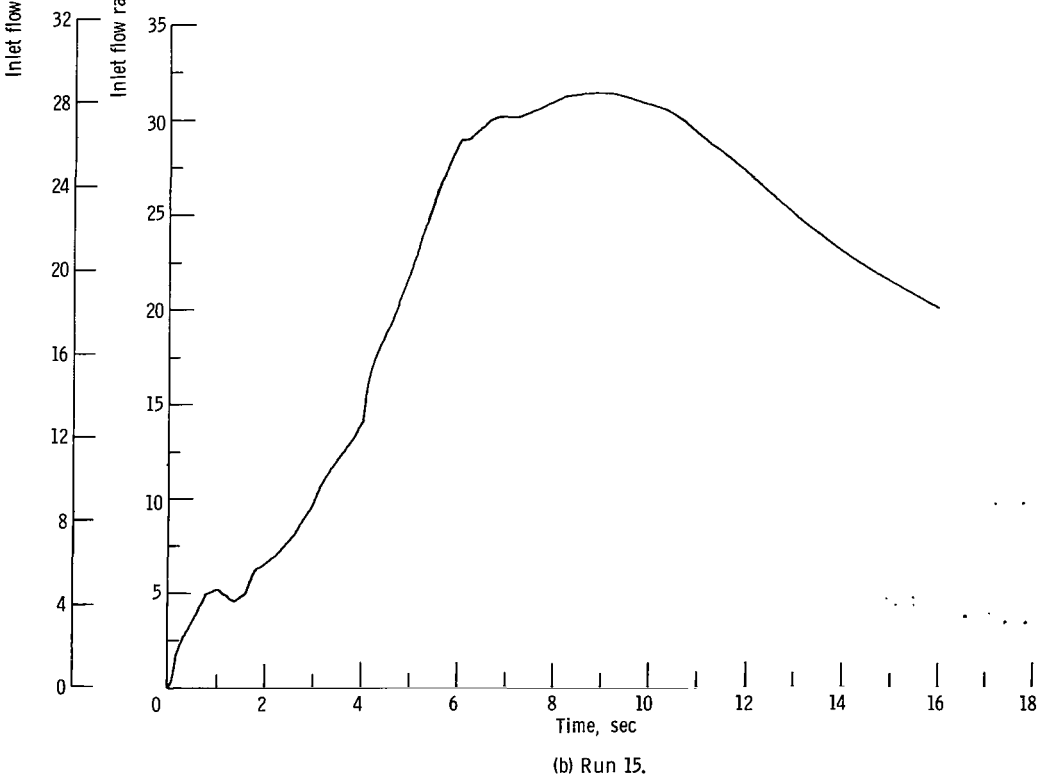

(b) Run 15.

Figure 8. - Flow rate at feedline inlet as function of time.

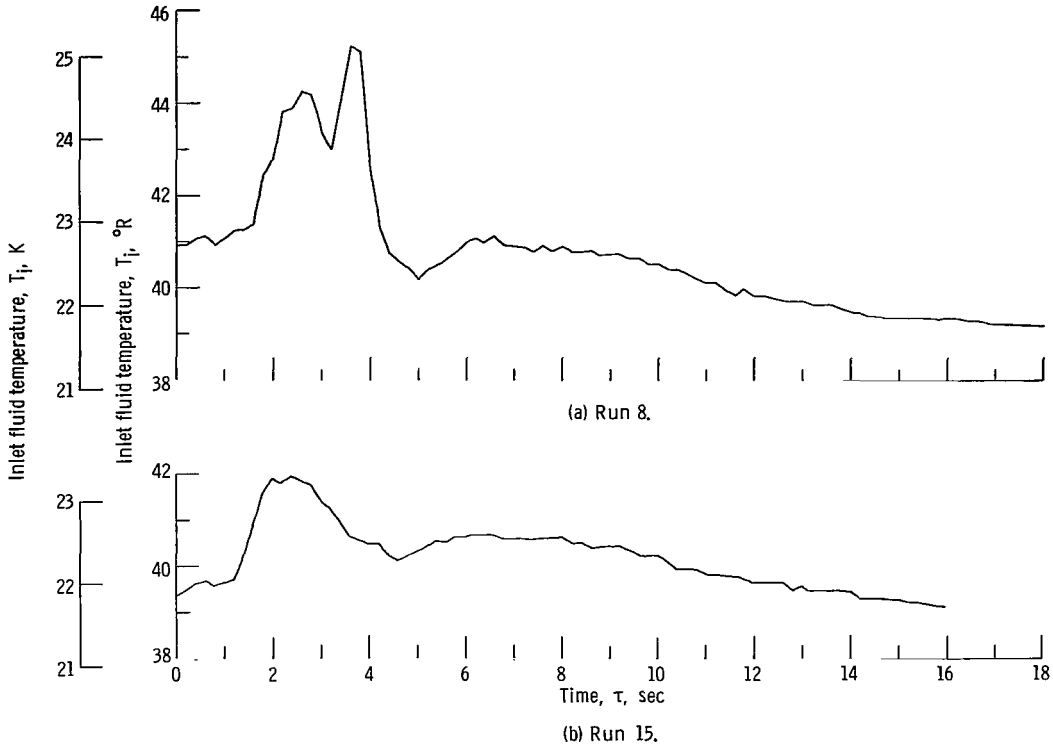

Figure 9. - Fluid temperature at feedline inlet against time.

As discussed in the section ANALYTICAL PROCEDURE, these time varying inlet conditions were used in the finite difference equations of continuity and energy to calculate hydrogen densities at the feedline outlet. As stated in the RESEARCH APPARATUS AND PROCEDURE section, the major difference between the two reported runs was in the flow-rate - time profiles. In run 15 the flow-rate change with respect to time at the feedline inlet (fig. 8(b)) was relatively smooth. And the measured and calculated density traces for run 15 (fig. 7(b)) were also relatively smooth. In run 8, however, the feedline inlet flow rate (fig. 8(a)) was oscillatory in the early part of the test; the corresponding density traces for run 8 (fig. 7(a)) have a similar oscillatory behavior.

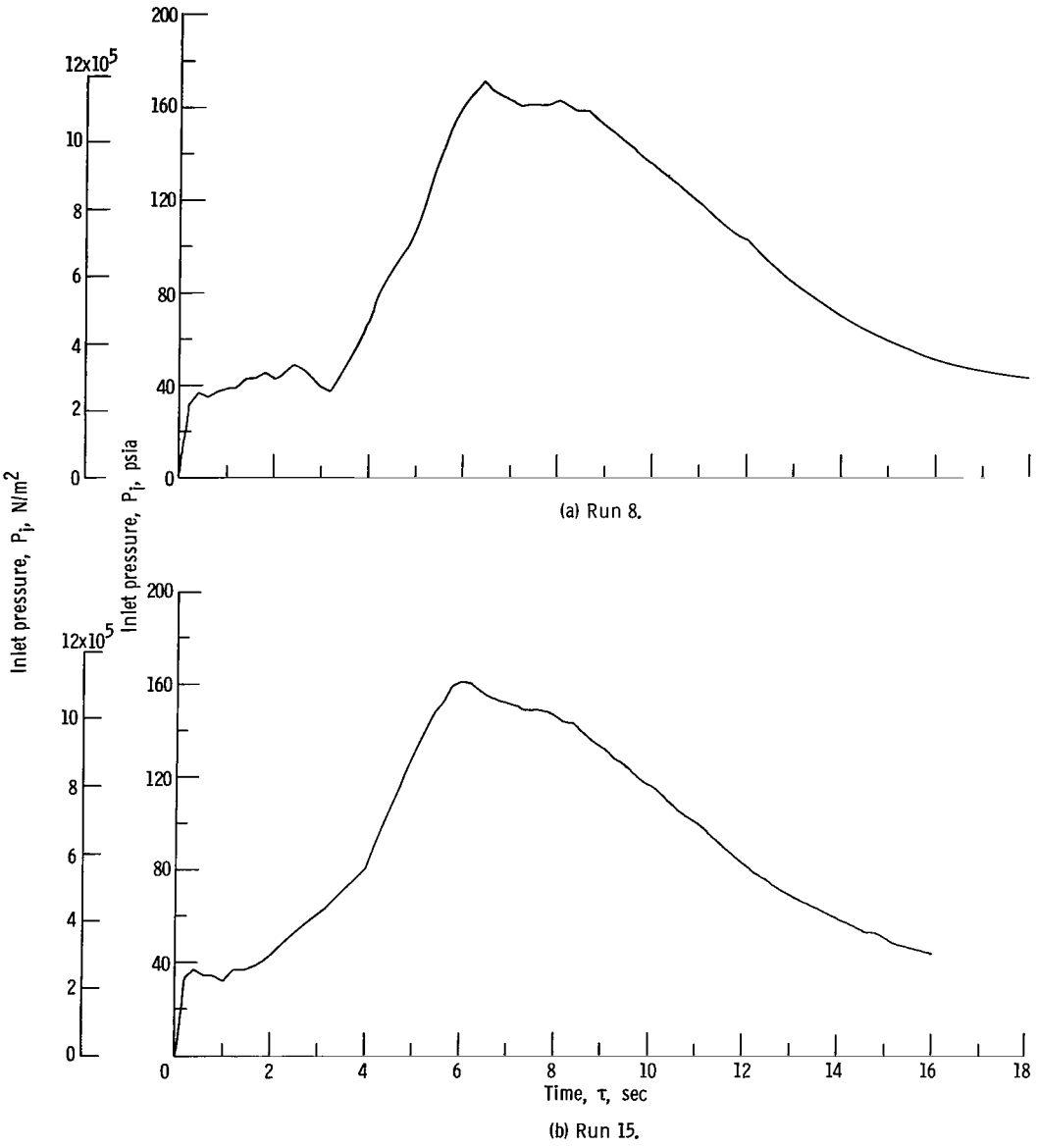

(a) Run 8.

(b) Run 15.

Figure 10. - Pressure at inlet to feedline as function of time.

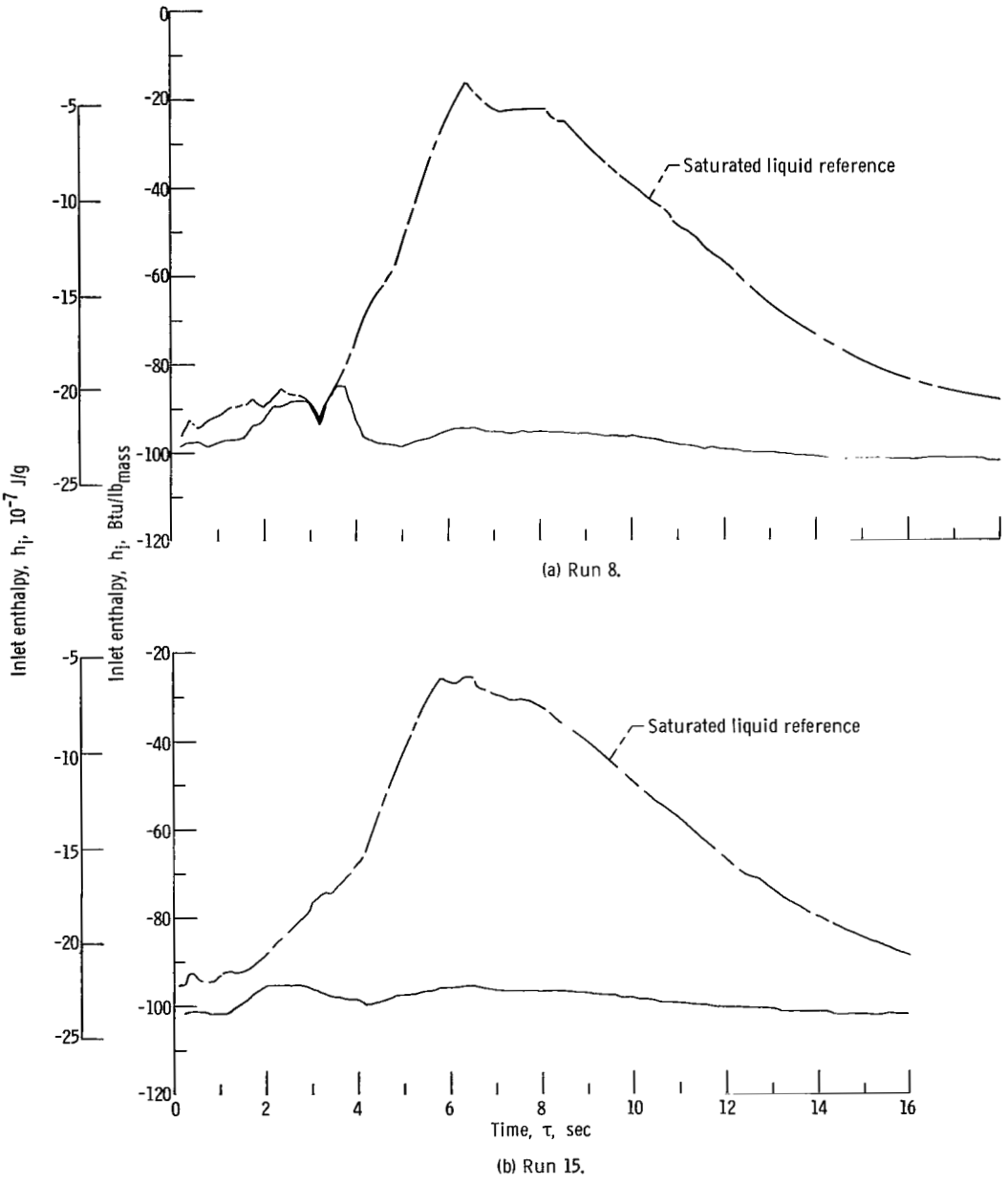

(a) Run 8.

(b) Run 15.

Figure 11. - Fluid enthalpy at feedline inlet against time.

CONCLUSION

For the runs presented herein, the local hydrogen densities measured with the capacitance density meter were in relatively close agreement with the corresponding calculated densities.

Most of the calculated and measured density values differed by less than ±15 percent of the full-scale (liquid hydrogen) density. For the most part, the calculated and measured densities for these tests were within the bands of uncertainty that resulted from (1) the inaccuracy of measurements that were used in the analytical density calculations and (2) the inaccuracy of the density meter.

It is concluded that the fluid density measurements made with this capacitance density meter were relatively accurate. Furthermore, this type of density meter could be used to measure two-phase and liquid-hydrogen densities with an accuracy that would be acceptable in many engineering applications.

Lewis Research Center,
National Aeronautics and Space Administration,
Cleveland, Ohio, September 11, 1968,
122-29-03-04-22.

APPENDIX - ERROR CONSIDERATIONS

The discrepancies between measured and calculated densities result from three different sources: (1) the errors of the density meter itself, (2) the errors in the data and the assumptions used to determine the calculated density, and (3) deviation of the experiment from the assumed conditions of thermal equilibrium and zero slip between the fluid phases. Each of these error sources are analyzed in the following sections of this appendix.

Error of Density Meter

The errors in the density meter correlation can be attributed to three different sources. The first is the ±1 percent uncertainty in the specific polarization in the Clausius-Mossotti equation. The second is the uncertainty in the calibration coefficient. The third and major source of error is the experimental uncertainty in measuring the matrix capacitance.

When $D = (C - C_{ref}) - (C_o - C_{ref})$ is substituted into the density equation (eq. (13)), the following error equation is derived:

$$\frac{d\rho}{\rho} = \left|\frac{dp}{p}\right| + \left|\frac{3\mathbb{A}_{T_c}}{D + 3\mathbb{A}_{T_c}} \frac{dD}{D}\right| + \left|\frac{3}{D + 3\mathbb{A}_{T_c}} d\mathbb{A}_{T_c}\right| \tag{A1}$$

But

$$\frac{3}{D + 3\mathbb{A}_{T_c}} \approx \frac{3}{3\mathbb{A}_{T_c}}$$

is a good approximation because $3\mathbb{A}_{T_c}$ is much larger than D. Therefore, the root mean square (rms) error is

$$\left(\frac{d\rho}{\rho}\right)_{rms} = \left[\left(\frac{dp}{p}\right)^2 + \left(\frac{d\mathbb{A}_{T_c}}{\mathbb{A}_{T_c}}\right)^2 + \left(\frac{dD}{D}\right)^2\right]^{1/2} \tag{A2}$$

The relative error in specific polarization p is about ±1 percent. Table I shows the consistency of p for six different experimenters. The ±1-percent variation in p shown in this table includes the random variation between experimenters and any nonrandom variation in the specific polarization due to density dependency.

The nonrandom variation is a result of p being a weak function of density. This variation indicates the degree to which hydrogen fluid does not obey the Clausius-Mossotti equation. Only the nonrandom varition in p will enter in the density meter equation error, because, here, p was assumed to be a constant. The individual calibration of the meter (i.e., the determination of the factor $\mathbb{A}_{T_c}$) should compensate for the experimenter's random error. Table I indicates little if any nonrandom error. Most of the variation appears to be random variation among the experimenters. Hust, et al., (ref. 10) report that the specific polarization is a function of density only. They give the relation between specific polarization (cm^3/gm) and density (gm/cm^3) by

$$\frac{1}{p} = 0.9957 - 0.09069\,\rho + 1.1227\,\rho^2 \tag{A2a}$$

From this relation, it can be shown that the maximum change in specific polarization is less than 0.2 percent. This value will be used in the error analysis.

The second error, the calibration uncertainty, appears as a variation in $\mathbb{A}_{T_c}$, the dielectric coefficient of the matrix. This error comes from two main sources. The determination of the density of the calibration fluid has some uncertainty. Also, the measure of the output capacitance of the system during calibration is affected by stray capacitance and instrumentation error.

Starting with the calibration equation for the dielectric coefficient of the matrix (eq. (15)), the rms calibration error is

$$\left(\frac{d\mathbb{A}_{T_c}}{\mathbb{A}_{T_c}}\right)_{rms} = \left[\left(\frac{d\left(C_{\rho_1} - C_{\rho_2}\right)}{\left(C_{\rho_1} - C_{\rho_2}\right)}\right)^2 + \left(\frac{d\left(\varepsilon_{\rho_1} - \varepsilon_{\rho_2}\right)}{\left(\varepsilon_{\rho_1} - \varepsilon_{\rho_2}\right)}\right)^2\right]^{1/2} \tag{A3}$$

But the error in the dielectric constant is related to the error in calibration density as follows:

$$d\varepsilon = \frac{p}{3}(\varepsilon + 2)^2\, d\rho \tag{A4}$$

where ε is an average value in the range of $d\varepsilon$. For simplicity, the approximation is $\varepsilon = \varepsilon_{\rho_2}$

But

$$d\rho = \left(\frac{\partial \rho}{\partial P}\right)_T dP + \left(\frac{\partial \rho}{\partial T}\right)_P dT \tag{A5}$$

If the condition is chosen to be a vacuum where $\rho_2 = 0$, then $\varepsilon_{\rho_2} = 1.0$, and the rms calibration error becomes

$$\frac{d\mathbb{A}_{T_c}}{\mathbb{A}_{T_c}} = \left[\left(\frac{d\left(C_{\rho_1} - C_{\rho_2}\right)}{\left(C_{\rho_1} - C_{\rho_2}\right)}\right)^2 + \left(\frac{3P}{\left(\varepsilon_{\rho_1} - 1\right)}\left(\frac{\partial \rho}{\partial P}\right)_T dP\right)^2 + \left(\frac{3P}{\left(\varepsilon_{\rho_1} - 1\right)}\left(\frac{\partial \rho}{\partial T}\right)_P dT\right)^2\right]^{1/2} \tag{A6}$$

Reasonable estimates of calibration measurement errors are $\pm\frac{1}{2}$ picofarad in capacitance, ±1 psia in pressure ($\pm 6.9 \times 10^3$ N/m^2); and $\pm 1^{\circ}$ R ($\pm 5/9$ K) in temperature. Therefore, the rms error due to the calibration is 2.27 percent.

The third error source is the uncertainty in measuring capacitance during an experimental run. This error is a result of changes in stray capacitance and also instrumentation error. The rms experimental error equation is

$$\left(\frac{dD}{D}\right)_{rms} = \left[\left(\frac{d(C - C_{ref})}{(C - C_{ref}) - (C_0 - C_{ref})}\right)^2 + \left(\frac{d(C_0 - C_{ref})}{(C - C_{ref}) - (C_0 - C_{ref})}\right)^2\right]^{1/2} \tag{A7}$$

Estimates of experimental measurement errors are $\pm\frac{1}{4}$ picofarad in $d(C_0 - C_{ref})$ and $\pm\frac{1}{2}$ picofarad in $d(C - C_{ref})$. Therefore, the rms error due to experimental measurement is 1.87 percent.

Total density measurement system rms error can now be found from equation (13). The total rms error is 2.98 percent. And this is the rms error of the density meter only.

Items That Affect Comparison of Calculated and Measured Two-Phase Densities

In the following paragraphs, four important items that could affect the comparison of calculated and measured two-phase hydrogen densities are considered. The first and

second items discussed deal with the possible differences in the calculated and measured densities due to nonuniformities in the temperatures and velocities of the phases in a two-phase flow mixture. The third and fourth items deal with possible inaccuracies in the calculated densities resulting from errors in experimental measurements and approximations used in the density calculations.

Thermodynamic nonequilibrium between phases. - The calculated two-phase densities in figure 7 are based on the assumption that the gas and liquid phases at the feedline outlet were in thermodynamic equilibrium. Heat-transfer experiments conducted with two-phase hydrogen flow (e.g., ref. 7) have shown that temperature differences may exist between the gas and liquid phases. With nonequilibrium conditions, it can be shown that the corresponding average two-phase density is always less than the equilibrium two-phase density.

For the test runs described in this report, no attempts were made to experimentally determine the degree of nonequilibrium in the two-phase flow. But it is likely that some differences did exist between the gas and liquid phase temperatures.

The effect of nonequilibrium on two-phase density is illustrated in figure 12. The nonequilibrium values of density are based on an assumed 10° R (5.56 K) superheat of the gas phase.

The equilibrium two-phase densities in figure 12 were calculated from the following equation:

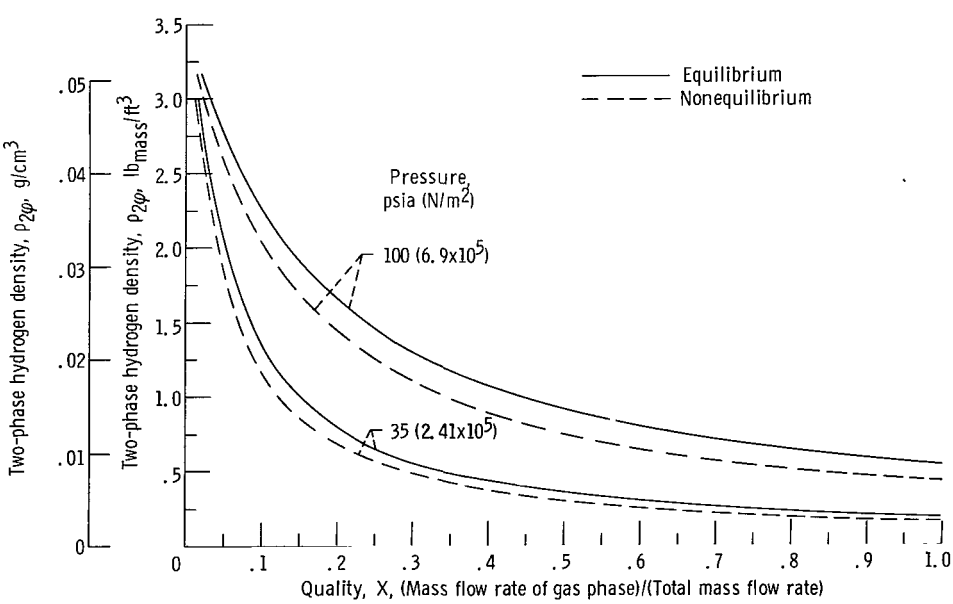

Figure 12. - Equilibrium and nonequilibrium two-phase densities against quality for pressures of 35 psia (2.41x10^5 N/m^2) and 100 psia (6.9x10^5 N/m^2). Nonequilibrium densities based on 10° R (5.56 K) superheat of gas phase.

$$\rho_{2\varphi} = \frac{1}{\frac{X}{\rho_{sg}} + \frac{1 - X}{\rho_{s\ell}}} \tag{A8}$$

The nonequilibrium two-phase densities were computed from the equation

$$\rho_{2\varphi,\,\text{noneq}} = \frac{1}{\frac{X - \epsilon}{\rho_{\text{superheated gas}}} + \frac{1 + \epsilon - X}{\rho_{s\ell}}} \tag{A9}$$

The fluid quality X in equation (A8) and (A9) is defined as

$$X = \frac{\text{Mass flow rate of gas phase}}{\text{Total mass flow rate}} = \frac{\dot{\omega}_g}{\dot{\omega}_g + \dot{\omega}_\ell} \tag{A10}$$

In equation (A9), ϵ is the fraction of the total liquid phase, which is not converted to gas because of nonequilibrium conditions. The value of ϵ depends on the pressure level and the amount of superheat of the gas phase. At a fixed pressure, ϵ is defined as follows:

$$\epsilon = \frac{X \int_{\Delta T_{\text{superheated gas}}} C_p \, dT}{(h_{sg} - h_{s\ell}) + \int_{\Delta T_{\text{superheated gas}}} C_p \, dT} \tag{A11}$$

Figure 12 shows the equilibrium and nonequilibrium two-phase densities as a function of quality X for pressures of 35 and 100 psia (2.41×10^5 and 6.9×10^5 N/m^2). The nonequilibrium traces in figure 12 are based on a 10° R (5.56 K) superheat of the gas phase.

The relative difference between equilibrium and nonequilibrium densities, that is, $(\rho_{2\varphi} - \rho_{2\varphi,\,\text{noneq}})/\rho_{2\varphi}$, increases as the equilibrium two-phase density decreases. For the pressure range from 35 to 100 psia (2.41×10^5 to 6.9×10^5 N/m^2) the maximum relative difference between equilibrium and nonequilibrium densities due to a 10° R (5.56 K) superheat of the gas phase is approximately -20 percent. And the maximum difference

expressed as a fraction of the full-scale (liquid hydrogen) density, that is, $(\rho_{2\varphi} - \rho_{2\varphi, \text{noneq}})/\rho_{sl}$, is about -6 percent.

The difference term $(\rho_{2\varphi} - \rho_{2\varphi, \text{noneq}})$ is approximately equal to the calculated density minus the measured density. This difference results when the gas and liquid phases are at different temperatures. Therefore, with nonequilibrium two-phase flow, the calculated densities would be expected to be less than the corresponding measured densities.

Velocity differences between phases. - The equilibrium density of a two-phase (gas-liquid) flow mixture is given by equations (A8) and (A10). By combining these equations, the equilibrium two-phase density can also be expressed as

$$\rho_{2\varphi} = \frac{\text{Total mass flow rate}}{\text{Total volumetric flow rate}} = \frac{\dot{\omega}_g + \dot{\omega}_l}{\frac{\dot{\omega}_g}{\rho_{sg}} + \frac{\dot{\omega}_l}{\rho_{sl}}} \tag{A12}$$

In this form, the density of a two-phase flow mixture is dependent only on the densities of the saturated gas and liquid phases and the flow rates of the phases. The density given by equation (A12) is commonly referred to as mixing-cup density.

Now consider a finite element of constant area passage with two-phase flow as illustrated in figure 13. From a static or stop action point of view, the average density of the flow mixture in the element of volume V (fig. 13) is given by

$$\rho_{2\varphi, s} = \frac{\text{Total mass in V}}{V} = \frac{m_g + m_l}{V} \tag{A13}$$

The mass of gas in volume element V is

$$m_g = \frac{\dot{\omega}_g L}{v_g} \tag{A14}$$

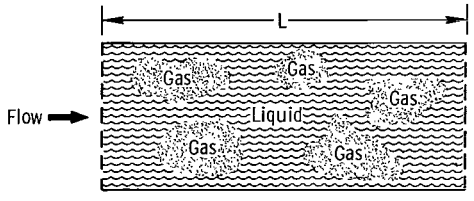

Figure 13. - Element of constant area passage with two-phase flow.

And the mass of liquid in volume element V is

$$m_l = \frac{\dot{\omega}_l L}{v_l} \tag{A15}$$

The volume of the element is

$$V = \frac{m_g}{\rho_{sg}} + \frac{m_l}{\rho_{sl}} = \frac{\dot{\omega}_g L}{v_g \rho_{sg}} + \frac{\dot{\omega}_l L}{v_l \rho_{sl}} \tag{A16}$$

Substituting the right side of equations (A14), (A15), and (A16) into equation (A13) and simplifying gives

$$\rho_{2\varphi,s} = \frac{\dot{\omega}_g + \left(\frac{v_g}{v_l}\right)\dot{\omega}_l}{\frac{\dot{\omega}_g}{\rho_{sg}} + \left(\frac{v_g}{v_l}\right)\frac{\dot{\omega}_l}{\rho_{sl}}} \tag{A17}$$

The density given by equation (A17) is the theoretical density of the two-phase fluid as measured by the density meter. The ratio v_g/v_l in equation (A17) is commonly referred to as slip. For slip equal to one, equation (A17) is identical to equation (A12). For $v_g/v_l \neq 1$, the density given by equation (A17) is different from that given by equation (A12), and $(\rho_{2\varphi} - \rho_{2\varphi,s})$ is the difference between calculated and measured two-phase densities due to nonuniform phase velocities.

In general, the average velocities of the individual phases of a two-phase flow mixture are not the same. For steady flow in a horizontal passage with heat addition, the slip v_g/v_l is usually greater than one. For the experiments described in this report, the flow was unsteady. And the slip at the capacitance transducer may have been greater than one at some times during these tests and less than one at other times.

The affect of slip on the density of two-phase hydrogen is shown in figure 14. (The curves in fig. 14 are based on an assumed constant pressure of 40 psia (2.76×10^5 N/m^2).) For slips ranging from 0.75 to 1.25, the maximum relative difference in measured and calculated densities at 40 psia (2.76×10^5 N/m^2), that is, $(\rho_{2\varphi} - \rho_{2\varphi,s})/\rho_{2\varphi}$, is approximately ±15 percent. And the maximum difference as a fraction of full-scale (liquid hydrogen) density $(\rho_{2\varphi} - \rho_{2\varphi,s})/\rho_{sl}$ is about ±5 percent. At pressures greater

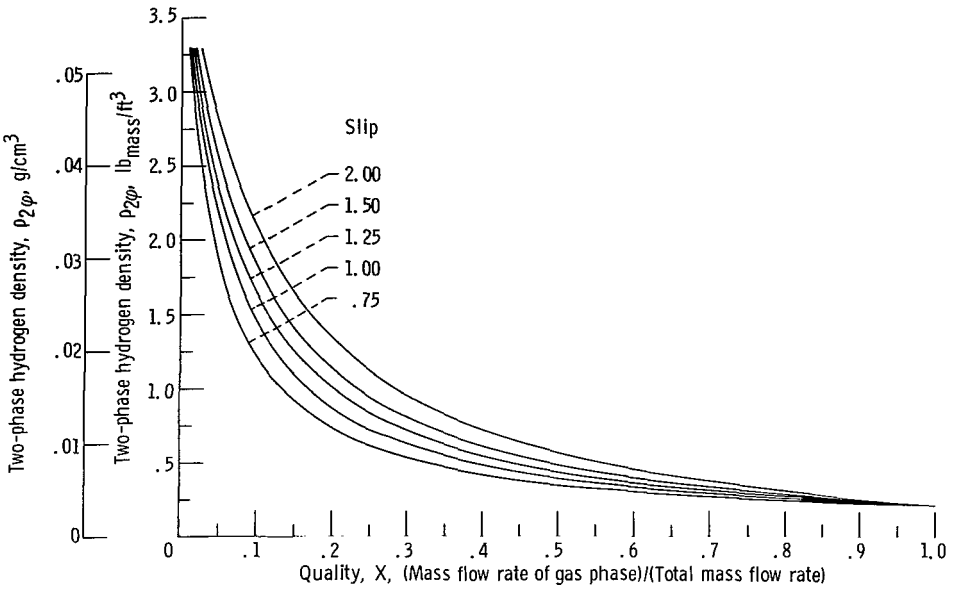

Figure 14. - Two-phase hydrogen density against quality with slip as parameter. (Data based on pressure of 40 psia (2.76×10^5 N/m^2).)

than 40 psia (2.76×10^5 N/m^2), the maximum difference is somewhat less than the previously stated values.

Accuracy of experimental measurements used in density calculations. - The estimated accuracies of the measured flow rates, pressures, fluid temperatures, and material temperatures are given in table II. Each of these measurements was used in the calculations to determine the density of hydrogen at the feedline outlet. In the discussion that follows, the effect of errors in these measurements on the calculated two-phase density at the feedline outlet is examined.

In the two-phase region, the local fluid density can be expressed as a function of the local pressure and enthalpy; that is,

$$\rho_{2\varphi} = \rho_{2\varphi}(P_o, h_o) \tag{A18}$$

And the total differential of the two-phase density is given by

$$d\rho_{2\varphi} = \left(\frac{\partial\rho_{2\varphi}}{\partial P_o}\right)_{h_o} dP_o + \left(\frac{\partial\rho_{2\varphi}}{\partial h_o}\right)_{P_o} dh_o \tag{A19}$$

If the time derivatives in equation (20) are neglected and uniform, steady flow is assumed, the enthalpy at the feedline outlet h_o can be written as

$$h_o = h_i + \frac{1}{\dot{\omega}} \int_{x_i}^{x_o} \dot{Q}'' \, dx = h_i + \frac{\dot{Q}_T}{\dot{\omega}} \tag{A20}$$

The total differential of the fluid enthalpy at the feedline outlet is

$$dh_o = \left(\frac{\partial h_o}{\partial \dot{\omega}}\right)_{\dot{Q}_T,\, h_i} d\dot{\omega} + \left(\frac{\partial h_o}{\partial \dot{Q}_T}\right)_{\dot{\omega},\, h_i} d\dot{Q}_T + \left(\frac{\partial h_o}{\partial h_i}\right)_{\dot{Q}_T,\, \dot{\omega}} dh_i \tag{A21}$$

The partial derivations in (A21) can also be written as

$$\left(\frac{\partial h_o}{\partial h_i}\right)_{\dot{Q}_T,\, \dot{\omega}} = 1 \tag{A22}$$

$$\left(\frac{\partial h_o}{\partial \dot{Q}_T}\right)_{\dot{\omega},\, h_i} = \frac{1}{\dot{\omega}} \tag{A23}$$

$$\left(\frac{\partial h_o}{\partial \dot{\omega}}\right)_{\dot{Q}_T,\, h_i} = -\frac{\dot{Q}_T}{(\dot{\omega})^2} \tag{A24}$$

If the right sides of equations (A21) to (A24) are substituted into (A19), the relative error in calculated two-phase density is given as

$$\frac{d\rho_{2\varphi}}{\rho_{2\varphi}} = \frac{1}{\rho_{2\varphi}} \left\{ \left| \left(\frac{\partial \rho_{2\varphi}}{\partial P_o}\right)_{h_o} dP_o \right| + \left| \left(\frac{\partial \rho_{2\varphi}}{\partial h_o}\right)_{P_o} \right| \left[\left| -\frac{\dot{Q}_T \, d\dot{\omega}}{(\dot{\omega})^2} \right| + \frac{|d\dot{Q}_T|}{\dot{\omega}} + |dh_i| \right] \right\} \tag{A25}$$

The relative error given by (A25) is dependent on the numerical values of P_o, $\rho_{2\varphi}$, $\dot{Q}_T$, and $\dot{\omega}$. And for fixed values of P_o, $\dot{Q}_T$, and $\dot{\omega}$, the relative error in calculated two-phase density approaches a maximum as $\rho_{2\varphi}$ approaches the saturated liquid density.

For P_o = 50 psia (3.45×10^5 N/m^2), $\dot{\omega}$ = 20 pounds mass per second (9.1 kg/sec), $\dot{Q}_T$ = 100 Btu per second (1.055×10^5 J/sec), and $\rho_{2\varphi}$ = 4 pounds mass per cubic foot (0.064 g/cm^3), the approximate numerical values of the partial derivations in equation (A25) are

$$\left(\frac{\partial \rho_{2\varphi}}{\partial P_o}\right)_{h_o} = 0.025 \frac{(lb_{mass})(in.^2)}{(lb_{force})(ft^3)} \qquad \left(5.8\times10^{-6} \frac{(g)(m^2)}{(N)(cm^3)}\right)$$

$$\left(\frac{\partial \rho_{2\varphi}}{\partial h_o}\right)_{P_o} = -0.32 \frac{lb_{mass}^2}{(Btu)(ft^3)} \qquad \left(2.22\times10^{-3} \frac{\frac{g}{cm^3}}{\frac{J}{g}}\right)$$

And from table II,

$$dP_o = \pm 2 \text{ psi } (1.38\times10^4 \text{ N/m}^2)$$

$$\frac{d\dot{\omega}}{\dot{\omega}} = \pm 0.02$$

From the specified accuracy of the fluid temperature measurements in table II, dh_i is about ± 0.75 Btu per pound mass ($\pm 1.76\times10^3$ J/kg). And, from the specified accuracy of the material temperature measurements, $d\dot{Q}_T$ was estimated to be about 3 Btu per second (3.165×10^3 J/sec).

Using these numerical values in equation (A25) results in a maximum relative error in $\rho_{2\varphi}$, due to possible inaccuracies in experimental measurements, of about 9 percent; that is, $d\rho_{2\varphi}/\rho_{2\varphi} \cong 0.09$.

Approximations used in determination of heat transfer rates. - As described in the section ANALYTICAL PROCEDURE the local rates of heat input to the fluid in the feedline were determined from changes in the measured local feedline temperatures with respect to time. These measured local temperatures, however, were outside metal surface temperatures.

Because of the nonsteady nature of these flow tests, the local feedline radial wall-temperature gradients were not constant during the experiments. In determining the heat-transfer rates, changes in the local radial wall-temperature gradients with time were not accounted for.

The effect of changes in these gradients on the calculated rates of heat transfer was investigated. For the tests reported herein, the maximum rate of change of the difference between the local measured outside surface temperature and the local average wall temperature was estimated to be less than $\pm 3^\circ$ R per second (5/3 K/sec); that is,

$$\left|\frac{d(T_w - T_M)}{d\tau}\right| < 3^o \frac{R}{sec} \qquad \left(\frac{\frac{5}{3} K}{sec}\right)$$

For this rate of change, the resulting maximum error in the calculated heat input rate was approximately ±5 percent. The maximum relative error in the calculated densities was also determined to be about ±5 percent. And the difference between calculated and measured densities in figure 7 may be as much as ±5 percent due to possible errors in the estimated heat inputs.

REFERENCES

1. Reardon, John E.: Full-Scale Nuclear Rocket Cold-Flow Test Facility and Research Apparatus. NASA TM X-1763, 1968.

2. Corruccini, R. J.: Dielectric Constant of Liquid Parahydrogen. Tech. Note 144, National Bureau of Standards, Apr. 1962.

3. Anon.: Problems Involved in Mass and Level Measurements Using Capacitance Sensors. Electronic Tech. Rep., Pioneer Central Div., Bendix Corp.

4. Hust, J. G.; Germann, F. E. E.; and Stewart, R. B.: A Compilation of the Dielectric Constants of Solid, Liquid, and Gaseous He, H_2, Ne, N_2, O_2, Air, CO_2, F_2, A, and CH_4 Below 300° K. Rep. 8252, National Bureau of Standards, Apr. 7, 1964.

5. Lauritzen, John I., Jr.; Corruccini, Robert J.; and Lonberger, S. T.: Reference Tables for Thermocouples. Circ. 561, National Bureau of Standards, Apr. 27, 1955.

6. Goldberg, Fredric N.; and Haferd, Angela M.: Numerical Procedures for Calculating Real Fluid Properties of Normal and Parahydrogen. NASA TN D-4341, 1968.

7. Chi, J. W. H.; and Vetere, A. M.: Two-Phase Flow During Transient Boiling of Hydrogen and Determination of Nonequilibrium Vapor Fractions. Advances in Cryogenic Engineering. Vol. 9. K. D. Timmerhaus, ed., Plenum Press, 1964, pp. 243-253.

8. Werner, W.; and Keesom, W. H.: Dielectric Constants of Hydrogen. K. Akad. Amsterdam, Proc., vol. 29, no. 1, 1926, pp. 34-43.

9. Guillien, R.: Dielectric Constant Near Melting Point. J. Physique Radium, vol. 1, Jan. 1940, pp. 29-33.

10. van Itterbeek, A.; and Spaepen, J.: Determination of Dielectric Constant of Liquid D. Physica, vol. 9, 1942, pp. 339-344.

11. Johns, H. E.; and Wilhelm, J. O.: Refractive Indices of Liquid Oxygen, Nitrogen, and Hydrogen. Can. J. Res., Sec. A, vol. 15, July 1937, pp. 101-108.

12. Maryott, Arthur A.; and Buckley, Floyd: Tables of Dielectric Constants and Electric Dipole Moments of Substances in the Gaseous State. Circ. 537, National Bureau of Standards, June 25, 1953.

13. Michels, A.; Sanders, P.; and Schipper, A.: Dielectric Constant of Hydrogen. Physica, vol. 2, Aug. 1935, pp. 753-756.

NATIONAL AERONAUTICS AND SPACE ADMINISTRATION
WASHINGTON, D. C. 20546

OFFICIAL BUSINESS

FIRST CLASS MAIL

POSTAGE AND FEES PAID
NATIONAL AERONAUTICS AN
SPACE ADMINISTRATION

POSTMASTER: If Undeliverable (Section 158 Postal Manual) Do Not Retur

"The aeronautical and space activities of the United States shall be conducted so as to contribute . . . to the expansion of human knowledge of phenomena in the atmosphere and space. The Administration shall provide for the widest practicable and appropriate dissemination of information concerning its activities and the results thereof."

—NATIONAL AERONAUTICS AND SPACE ACT OF 1958

NASA SCIENTIFIC AND TECHNICAL PUBLICATIONS

TECHNICAL REPORTS: Scientific and technical information considered important, complete, and a lasting contribution to existing knowledge.

TECHNICAL NOTES: Information less broad in scope but nevertheless of importance as a contribution to existing knowledge.

TECHNICAL MEMORANDUMS: Information receiving limited distribution because of preliminary data, security classification, or other reasons.

CONTRACTOR REPORTS: Scientific and technical information generated under a NASA contract or grant and considered an important contribution to existing knowledge.

TECHNICAL TRANSLATIONS: Information published in a foreign language considered to merit NASA distribution in English.

SPECIAL PUBLICATIONS: Information derived from or of value to NASA activities. Publications include conference proceedings, monographs, data compilations, handbooks, sourcebooks, and special bibliographies.

TECHNOLOGY UTILIZATION PUBLICATIONS: Information on technology used by NASA that may be of particular interest in commercial and other non-aerospace applications. Publications include Tech Briefs, Technology Utilization Reports and Notes, and Technology Surveys.

Details on the availability of these publications may be obtained from:

SCIENTIFIC AND TECHNICAL INFORMATION DIVISION

NATIONAL AERONAUTICS AND SPACE ADMINISTRATION

Washington, D.C. 20546